



A phase-field model for strain localization analysis in softening elastoplastic materials

Giuseppe Giambanco*, Emma La Malfa Ribolla

Department of Civil, Environmental, Aerospace Engineering and Materials (DICAM) University of Palermo, Viale delle Scienze Ed. 8, Palermo 90128, Italy



ARTICLE INFO

Article history:

Received 30 October 2018

Revised 28 February 2019

Available online 5 April 2019

Keywords:

Phase-field

Elastoplasticity

Softening

Strain localization

ABSTRACT

The present paper deals with the localization of strains in those structures consisting of materials exhibiting plastic softening response. It is assumed that strain localization develops in a finite thickness band separated from the remaining part of the structure by weak discontinuity surfaces. In view of the small thickness of the band with respect to the dimensions of the structure, the interphase concept is used for the mechanical modeling of the localization phenomenon. We propose a formulation for the quasi-static modeling of strain localization based on a phase-field approach. In this sense, the localization band is smeared over the volume of the structure and a smooth transition between the fully broken and the sound material phases is introduced. The mechanical performance of the model is illustrated for the case of uniaxial tensile test, discussing the instability of the force-displacement response, and for the case of three-point bending test, comparing the analytical results with the experimental ones.

© 2019 Elsevier Ltd. All rights reserved.

1. Introduction

Failure of structural components constituted by rate-independent strain softening materials is characterized by the localization of strains in relatively narrow zones, which gradually transform in stress free cracks, usually called cracks bands, shear bands or simply localization bands. At the microscopic level this behavior can be explained as the evolution of micro-voids and micro-cracks which, during the loading process, interact and join together up to the formation of the macroscopic surface of fracture.

Theoretical and computational modeling of strain localization is a challenging task. In the pioneering work of Rudnicki and Rice (1975), later generalized by Ottosen and Runesson (1991), the onset of localized deformations is considered as the result of an instability in the macroscopic constitutive description of inelastic deformation and corresponds to a bifurcation problem, i.e. the incremental equations governing the equilibrium show a loss of uniqueness and an alternative deformation mode associated to the evolution of the localization band is admitted.

A crucial point of the theoretical treatment of the localization problem is the evolutive kinematic description of the strain band. This can be approached in three different forms (Jirásek, 2001):

- Considering the middle surface of the narrow localization zone as a singularity surface respect to the displacement field;
- Admitting the presence of a finite thickness band, separated from the remaining part of the structure by weak discontinuities surfaces, across which the displacement is continuous but where the strain state has a jump;
- Smearing the plastic strain band on the surrounding volume regularizing the displacement field, which becomes continuous and differentiable, leading, then, to a continuous strain field.

The first approach is typical of elastic fracture mechanics and the singularity surface represents the stress free crack. Usually this approach corresponds numerically to interface elements inserted between finite elements, where standard shape functions are enriched by special discontinuous functions (Moës et al., 1999).

The second approach considers the fracture process zone as a sort of zero-thickness interface characterized by its own constitutive law, which relates the contact tractions to the displacement jumps across the interface (Giambanco et al., 2014; Spada et al., 2015; Giambanco et al., 2018). The jump of the displacement component along the normal direction to the interface layer constitutes the crack opening (mode I), while jumps of the displacement components in the tangential direction represent the crack sliding (mode II). In a more sophisticated model, the localization analysis can be performed accounting for the internal stresses in the band. In this case, the interphase concept can be adopted and it consists of a thin layer separated from the sound material by two interfaces, where a specific kinematic distinguishes contact and

* Corresponding author.

E-mail address: giuseppe.giambanco@unipa.it (G. Giambanco).

Nomenclature*Greek Symbols*

α	Reciprocal of half thickness of the localization band
β	Ratio between the yield strain and the ultimate strain
β	Fraction volume of the localization band
δ	Micro-strain vector associated to the phase-change
ζ	Micro-stress
$\hat{\epsilon}$	Regular part of the strain state
χ	Static internal variable energetically conjugated to ξ
δ_{Σ_b}	Line Dirac delta function
γ	Mumford-Shah type functional
Φ	Activation function
π	Micro-force
ψ	Helmholtz free energy density
ρ	Distance function to the surface Σ_b
φ	Beam curvature
ξ	Kinematic internal variable
σ	Stress tensor
ϵ	Strain tensor
λ	Lagrangian multiplier

Roman Symbols

g	Strain jump
L	Acoustic tensor
m	Polarization vector
n	Surface normal
D	Intrinsic dissipation
f	Volume force
t	Surface tractions
u	Displacement vector
E	Fourth-order stiffness tensor
A	Area of the cross section
B	Beam thickness
c	Crack phase-field variable
D	Intrinsic dissipation density
E	Young's modulus
F	Point load
H	Beam depth
h	Hardening/softening parameter
I	Inertia of the cross section
L	Lagrangian functional
l	Bar or beam span length
R	Ramp function
S	Slope of the linear softening branch
w_b	Length of the localization band

Superscripts

<i>c</i>	Contact component
<i>e</i>	Elastic part
<i>i</i>	Internal component
<i>p</i>	Plastic part
<i>ph</i>	Phase-change part
<i>s</i>	Symmetric part
<i>t</i>	Tangent

Subscripts

0	Threshold value
b	Localization band
dis	Dissipative
f	Ultimate
s	Material outside the localization band
t	Tensile threshold value

Other Symbols

\mathcal{H}	Heaviside step function
\mathcal{I}	Indefinite integral
\mathcal{II}	Indefinite double integral

internal strains (Giambanco and Mróz, 2001; Giambanco et al., 2012; Fileccia Scimemi et al., 2014).

Finally, the third approach makes use of advanced constitutive models for the strain-softening material, which belong to the class of enriched continua theories. This is the case of the nonlocal or high-order continua, which typically introduce a material internal length, considered as a constitutive parameter, directly related to the width of the localization band (Benvenuti et al., 2002; Borino and Polizzotto, 2007).

In the last two decades, the description of crack formation and evolution has been developed in the ambit of continuum mechanics making use of the phase-field method, where the *order parameter*, in this context called *crack phase-field*, describes the smooth transition between the fully broken and the sound material phases.

A number of research works refers to the case of brittle fracture and they arise from the variational formulation of the equilibrium problem for a cracking solid formulated by Francfort et al. (2008). The principal aspect is the geometric approximation of the discontinuity surface by a regularized crack surface functional, which depends on the crack phase-field. The phase-field variable is considered as an additional degree of freedom for the enriched solid and its static counterpart appears in the equilibrium equation associated to.

The phase-field description of the brittle fracture has been developed in a thermodynamic consistent manner by Miehe et al. (2010) and numerically implemented for the static and dynamic case (Borden et al., 2012), using the finite element method, with the advantage that no special element is required to model cracks initiation, branching and coalescence in structures, where no prior knowledge of the crack paths is available.

Further developments have regarded the simulation of cohesive fracture (Verhoosel and de Borst, 2013; Feng and Wu, 2018), ductile fracture (Ambati et al., 2015; Alessi et al., 2018) and the shear localization in elasto-plastic material (Freddi and Royer Carfagni, 2016).

The present paper, in line with the cited works, aims to develop a thermodynamically consistent formulation of the localization problem in quasi-static regime adopting the phase-field approach to replace the discrete interfaces between the localized and not localized zone with diffuse interfaces.

In the cited papers, the strain localization occurrence, or the formation and propagation of fracture, is related to the competition of different physical mechanisms of deformation and the mechanical modeling requires the identification of a driving force, which is an energy, and of its threshold value, i.e. the energetic barrier to overcome (Palmer and Rice, 1973). The mathematical problem is regularized introducing the phase-field variable or order parameter, which evolves along the deformation process, leading to the decreasing of the driving force and the development of the instantaneous dissipation, which depends on the rate of the phase-field and its gradient.

The approach here proposed starts from the idea of distributing the dissipated energy, competing to the strain localization volume, on the whole volume of the structure, through a weak Dirac delta function of the phase-field variable. At the same time, the narrow volume zone where strain localization occurs is mechanically modeled as an interphase. This source idea leads to an original contact strain homogenization, with the continuity of the internal strains. The introduction of the phase-field variable enriches

the solid kinematics, in this sense the proposed formulation can be categorized in the class of the regularized models, where the plastic band is smeared on its around volume, with the order parameter assuming the unit value in middle surface of the band, geometrically coinciding with the interphase surface, and zero value sufficiently far from the same band. The length over the phenomenon diffuses is assumed to be a constitutive parameter, coinciding with the band thickness.

The paper is structured as follows. The fundamental concepts regarding the strain localization are reported in the next section. In order to particularize the mechanical problem to the case of strain softening materials, Section 3 illustrates the linear softening model whose constitutive equations (state laws, instantaneous dissipation, flow rules and loading/unloading conditions) are derived in a thermodynamically consistent manner. Section 4 is devoted to develop the strain localization problem in plasticity, assuming that the plastic strains concentrate in a narrow zone of finite thickness, that is generally small, if compared to typical dimension of the structure. The concept of zero-thickness interface is introduced and the mechanical treatment of the problem follows the approach presented by Simo et al. (1993).

The proposed model for strain localization is presented in Section 5 adopting the interphase concept, where the total strain is assumed constant along the thickness, assuming the band thickness sufficiently small in comparison to the structure dimension. Adopting the phase-field model, the discontinuity of the deformation is regularized, then, the development of the materials constitutive equations is given following the standard thermodynamic approach, with the new mechanical quantities associated to the phase change.

The model is finally applied to two examples, regarding a tensile test on a mortar bar and a three-point bending test on a concrete beam.

2. The strain localization problem

Let us consider in the Euclidean space \mathbb{R}^3 , referred to the orthonormal frame $(0, \mathbf{e}_1, \mathbf{e}_2, \mathbf{e}_3)$, a solid body Ω constituted by an elasto-plastic, strain-softening material (Fig. 1). The boundary of the structure is divided in two parts Γ_u and Γ_t , where the kinematic and loading conditions are specified, respectively.

Under severe loading conditions, strains concentrate in narrow zones, represented macroscopically by localized bands Ω_b , with thickness w_b , separated from the remaining part Ω_s by weak discontinuity surfaces Σ^+ , Σ^- (Fig. 1 (a)). Across these surfaces, the displacement field is continuous but the strain field exhibits a jump. In particular, following the pioneering work of Rudnicki and

Rice (1975), later generalized by Ottosen and Runesson (1991), we assume that:

- the tractions rate are continuous at the interfaces:

$$[[\dot{\boldsymbol{\sigma}}]] \cdot \mathbf{n}_b = (\dot{\boldsymbol{\sigma}}_b - \dot{\boldsymbol{\sigma}}_s) \cdot \mathbf{n}_b = \mathbf{0}, \quad (1)$$

where the symbol $[[\cdot]]$ represents the discontinuity of the enclosed quantity, $\dot{\boldsymbol{\sigma}}_b$ and $\dot{\boldsymbol{\sigma}}_s$ are the stress rates in the localized and in the non-localized regions, respectively, \mathbf{n}_b is the versor normal to the middle surface of the localization band;

- the strains rate are discontinuous at the interfaces:

$$[[\dot{\boldsymbol{\varepsilon}}]] = \dot{\boldsymbol{\varepsilon}}_s - \dot{\boldsymbol{\varepsilon}}_b = (\dot{\mathbf{g}} \otimes \mathbf{n}_b)^s, \quad (2)$$

with $\dot{\boldsymbol{\varepsilon}}_s$ and $\dot{\boldsymbol{\varepsilon}}_b$ representing the strain rates in the two volume parts, $\dot{\mathbf{g}}$ the vector measuring the strain jump and where the apex s indicates the symmetric part of the tensor.

The strain jump provides the information about the localization mode. Introducing the so-called polarization vector, defined as

$$\mathbf{m} = \frac{\dot{\mathbf{g}}}{|\dot{\mathbf{g}}|} = \frac{\dot{\mathbf{g}}}{\dot{g}}, \quad (3)$$

where the symbol $|\cdot|$ indicates the modulus of the enclosed vector, the angle between the unit vectors \mathbf{m} and \mathbf{n}_b characterizes the failure mode, since the condition $\mathbf{m} \equiv \mathbf{n}_b$ corresponds to the tensile splitting (mode I), the condition $\mathbf{m} \cdot \mathbf{n}_b = 0$ corresponds to the shear slip (mode II) and the remaining conditions represent the mix mode failures.

Since the strain rates are different in the two regions, generally the tangent stiffness tensor can be different as well, thus

$$\dot{\boldsymbol{\sigma}}_b = \mathbf{E}_b^t : \dot{\boldsymbol{\varepsilon}}_b, \quad (4a)$$

$$\dot{\boldsymbol{\sigma}}_s = \mathbf{E}_s^t : \dot{\boldsymbol{\varepsilon}}_s, \quad (4b)$$

with \mathbf{E}_b^t and \mathbf{E}_s^t representing the tangent stiffnesses in the localized and in the non-localized regions, respectively. The continuity condition (1) can be rewritten including the constitutive Eqs. (4a) and (4b) and taking into account Eqs. (2) and (3):

$$\dot{\mathbf{g}}(\mathbf{n}_b \cdot \mathbf{E}_b^t \cdot \mathbf{n}_b) \cdot \mathbf{m} = \mathbf{n}_b \cdot (\mathbf{E}_b^t - \mathbf{E}_s^t) : \dot{\boldsymbol{\varepsilon}}_s. \quad (5)$$

At the incipient formation of the weak discontinuity or bifurcation point, the tangent stiffnesses in the localized and non-localized regions are the same $\mathbf{E}_b^t = \mathbf{E}_s^t = \mathbf{E}^t$, therefore Eq. (5) reduces to

$$(\mathbf{n}_b \cdot \mathbf{E}^t \cdot \mathbf{n}_b) \cdot \mathbf{m} = \mathbf{L} \cdot \mathbf{m} = \mathbf{0}, \quad (6)$$

where the second order tensor \mathbf{L} is called localization or acoustic tensor. The Eq. (6), corresponding to the continuous bifurcation,

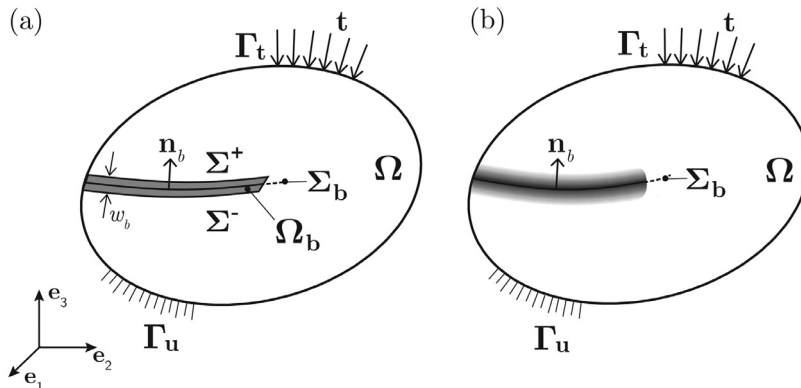


Fig. 1. Localized deformation in a strain softening material distinguishing (a) sharp localization band included in a solid Ω (b) diffusive localization band included in a solid Ω .

admits a non-trivial solution \mathbf{m} for a direction \mathbf{n}_b if the acoustic tensor is singular:

$$\det(\mathbf{L}) = 0, \quad (7)$$

therefore the onset of strain localization coincides to the loss of ellipticity of the governing differential equations. After plastic band localization, the two portions of the body can be assumed as two different materials, having their own tangent stiffness matrices. This condition is even called elastic/plastic bifurcation or *discontinuous bifurcation* and the strain jump has to satisfy Eq. (5).

3. Thermodynamic assumptions

The constitutive laws for the elastoplastic material can be derived in a thermodynamic consistent manner, assuming the following form of the Helmholtz free energy:

$$\psi = \psi^e + \psi^i = \frac{1}{2}(\boldsymbol{\varepsilon} - \boldsymbol{\varepsilon}^p) : \mathbf{E} : (\boldsymbol{\varepsilon} - \boldsymbol{\varepsilon}^p) + \frac{1}{2} h \xi^2, \quad (8)$$

where ψ^e and ψ^i are the elastic and internal components of the free energy, respectively. In the Eq. (8) $\boldsymbol{\varepsilon}^p$ is the inelastic deformation, ξ the kinematic internal variable associated to the plastic mechanism, \mathbf{E} the fourth order elastic tensor and h the hardening/softening parameter. The second principle of thermodynamics, taking into account the balance equation (first principle), can be written as the Clausius–Duhem inequality, which, for an isothermal purely mechanical evolutive process, reads

$$\dot{D}^p = \boldsymbol{\sigma} : \dot{\boldsymbol{\varepsilon}} - \dot{\psi} = \boldsymbol{\sigma} : \dot{\boldsymbol{\varepsilon}}^p - \chi \dot{\xi} \geq 0 \quad (9)$$

where, using classical arguments, the following relations have been considered

$$\boldsymbol{\sigma} = \frac{\partial \psi^e}{\partial \boldsymbol{\varepsilon}^e}, \quad \chi := \frac{\partial \psi^i}{\partial \xi}. \quad (10)$$

being $\boldsymbol{\sigma}$ the stress state and χ the static variable, energetically conjugated to the internal variable ξ .

The inelastic dissipative mechanism is driven by the activation function, defined in the space of the static variables in the following general form:

$$\Phi^p(\boldsymbol{\sigma}, \chi) = f(\boldsymbol{\sigma}, \chi) - \sigma_0 \leq 0, \quad (11)$$

where $f(\boldsymbol{\sigma}, \chi)$ is convex function, positively homogeneous of degree one and σ_0 is the yield stress.

Assuming that the model belongs to the class of the generalized standard materials, the complete set of evolutive constitutive relations can be derived by a specific maximum dissipation theorem, i.e. by maximization of the functional (9) under the admissibility condition (11). Adopting the Lagrange multiplier method, this maximization problem is equivalent to the following unconstrained stationarity problem:

$$\min_{\dot{\lambda}^p} \max_{\boldsymbol{\sigma}, \chi} L(\dot{\boldsymbol{\varepsilon}}^p, \dot{\xi}, \dot{\lambda}^p) = \boldsymbol{\sigma} : \dot{\boldsymbol{\varepsilon}}^p - \chi \dot{\xi} - \dot{\lambda}^p \Phi^p(\boldsymbol{\sigma}, \chi), \quad (12)$$

which provides the following flow rules

$$\frac{\partial L}{\partial \boldsymbol{\sigma}} = \mathbf{0} \rightarrow \dot{\boldsymbol{\varepsilon}}^p = \dot{\lambda}^p \frac{\partial \Phi^p}{\partial \boldsymbol{\sigma}} \rightarrow \dot{\boldsymbol{\varepsilon}}^p = \dot{\lambda}^p \frac{\partial f}{\partial \boldsymbol{\sigma}}, \quad (13a)$$

$$\frac{\partial L}{\partial \chi} = \mathbf{0} \rightarrow \dot{\xi} = -\dot{\lambda}^p \frac{\partial \Phi^p}{\partial \chi} \rightarrow \dot{\xi} = -\dot{\lambda}^p \frac{\partial f}{\partial \chi}, \quad (13b)$$

with the Kun–Tucker or loading/unloading conditions

$$\Phi^p(\boldsymbol{\sigma}, \chi) \leq 0, \quad \dot{\lambda}^p \geq 0, \quad \Phi^p \dot{\lambda}^p = 0. \quad (14)$$

Substituting the flow rules (13a) and (13b) in the instantaneous dissipation (9), using the Euler's homogenous functions theorem and considering the expression (11) as equality (i.e. the plastic mechanism is activated), we obtain

$$\dot{D}^p = \sigma_0 \dot{\lambda}^p \geq 0. \quad (15)$$

4. Localization in plasticity

The strain localization problem is here specialized for the case of a structure constituted by an elastoplastic material exhibiting strain softening. Firstly, we develop the problem with reference to the first approach mentioned in Section 1, i.e. considering the middle surface of the narrow localization zone as a singularity surface with respect to the displacement field. The hypotheses are:

- the thickness of the plastic band is small if compared to the characteristic dimensions of the structure;
- the inelastic strains in the band are derived from the displacement jump across opposite sides of the localization band.

According to these hypotheses, the thin layer of the localization band collapse in a zero-thickness interface, coinciding with its middle surface Σ_b . The strain state can be represented by a regular part $\hat{\boldsymbol{\varepsilon}}$ and a discontinuous part, concentrated at the zero-thickness interface:

$$\boldsymbol{\varepsilon} = \hat{\boldsymbol{\varepsilon}} + ([\mathbf{u}] \otimes \mathbf{n}_b)^s \delta_{\Sigma_b}, \quad (16)$$

where $[\mathbf{u}] = \mathbf{u}^+ - \mathbf{u}^-$ and δ_{Σ_b} is the line Dirac delta function associated to the smooth surface Σ_b , embedded in the three-dimensional body Ω , defined in the Euclidean space \mathbb{R}^3 . The line Dirac delta function is a distribution such that for any test function $f(\mathbf{x})$, infinitely differentiable and compactly supported,

$$\int_{\Omega} \delta_{\Sigma_b}(\mathbf{x}) \cdot f(\mathbf{x}) dV = \int_{\Sigma_b} f(\mathbf{x}(\mathbf{s})) dS, \quad (17)$$

where the $\mathbf{x}(\mathbf{s})$ is a spatial point on the surface Σ_b , where the curvilinear coordinate \mathbf{s} is defined (Fig. 2). For practical application, according to Zhang and Zheng (2012), the line delta function is defined as

$$\delta_{\Sigma_b}(\mathbf{x}) = \frac{1}{w_b(\mathbf{x})} \delta_{\Sigma_b}(\rho(\mathbf{x})), \quad (18)$$

where $\rho(\mathbf{x})$ is the distance function to the surface Σ_b . The continuity of contact tractions at the interface (1), considering the state law (10)₁, the flow rule (13a) and the definition of the total strain (16), can be rewritten in the following form:

$$[\boldsymbol{\sigma}] \cdot \mathbf{n}_b = \mathbf{E} : \left[\hat{\boldsymbol{\varepsilon}} + ([\mathbf{u}] \otimes \mathbf{n}_b)^s \delta_{\Sigma_b} - \dot{\lambda}^p \frac{\partial f}{\partial \boldsymbol{\sigma}} \right] \cdot \mathbf{n}_b = \mathbf{0}. \quad (19)$$

The above continuity condition holds only if the plastic multiplier is also composed by a regular and discontinuous part, i.e.

$$\dot{\lambda}^p = \dot{\lambda}_s^p + \dot{\lambda}_b^p \delta_{\Sigma_b}. \quad (20)$$

Therefore, the stress increment results in

$$\dot{\boldsymbol{\sigma}} = \mathbf{E} : \left\{ \hat{\boldsymbol{\varepsilon}} - \dot{\lambda}_s^p \frac{\partial f}{\partial \boldsymbol{\sigma}} + \left[([\mathbf{u}] \otimes \mathbf{n}_b)^s - \dot{\lambda}_b^p \frac{\partial f}{\partial \boldsymbol{\sigma}} \right] \delta_{\Sigma_b} \right\}. \quad (21)$$

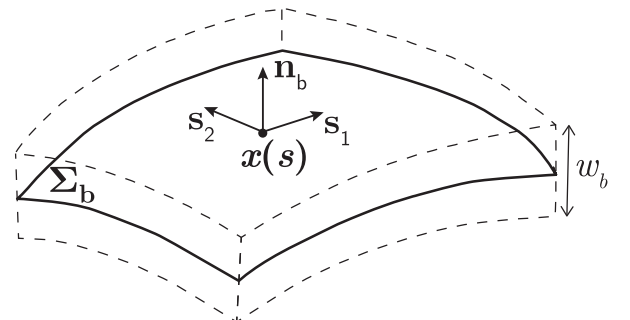


Fig. 2. Localization band Σ_b collapsed in a zero thickness interphase.

In view of this result, we can distinguish two different situations: the case of non localized deformation, i.e. $\dot{\lambda}_b^p = 0$, which gives

$$\dot{\boldsymbol{\sigma}} = \mathbf{E} : \left(\dot{\boldsymbol{\varepsilon}} - \dot{\lambda}_s^p \frac{\partial \mathbf{f}}{\partial \boldsymbol{\sigma}} \right), \quad \llbracket \dot{\mathbf{u}} \rrbracket = 0, \quad \dot{\lambda}^p = \dot{\lambda}_s^p, \quad (22)$$

thus the total strain corresponds to the regular part and the elastic strain is defined in the classical way as $\boldsymbol{\varepsilon}^e = \boldsymbol{\varepsilon} - \boldsymbol{\varepsilon}^p$.

In the case of localized deformation, we consider that the material inside the band responds plastically while in the remaining volume it responds elastically (elasto/plastic bifurcation, $\dot{\lambda}_s^p = 0$, $\dot{\lambda}_b^p \neq 0$). From Eq. (21), we obtain that the regular part of the strain increment coincides with the elastic strain increment, the plastic strain in the band is responsible for the discontinuous part of the strain increment and the plastic multiplier is a discontinuous function, which assume the value $\dot{\lambda}_b^p$ on the surface Σ_b :

$$\dot{\boldsymbol{\sigma}} = \mathbf{E} : \dot{\boldsymbol{\varepsilon}}, \quad (\llbracket \dot{\mathbf{u}} \rrbracket \otimes \mathbf{n}_b)^s = \dot{\lambda}_b^p \frac{\partial \mathbf{f}}{\partial \boldsymbol{\sigma}}, \quad \dot{\lambda}^p = \dot{\lambda}_b^p \delta_{\Sigma_b}. \quad (23)$$

In order to complete the analysis, the regular and the discontinuous part of the plastic multipliers remain to be determined, by enforcing the plastic consistency condition:

$$\dot{\Phi} = \frac{\partial \mathbf{f}}{\partial \boldsymbol{\sigma}} : \dot{\boldsymbol{\sigma}} + \frac{\partial \mathbf{f}}{\partial \chi} \dot{\chi} = 0 \quad (24)$$

which, considering Eqs. (21), (10)₂ and (13b) is computed as

$$\begin{aligned} \dot{\Phi} = \frac{\partial \mathbf{f}}{\partial \boldsymbol{\sigma}} : \mathbf{E} : \left(\dot{\boldsymbol{\varepsilon}} - \dot{\lambda}_s^p \frac{\partial \mathbf{f}}{\partial \boldsymbol{\sigma}} \right) - \left(\frac{\partial \mathbf{f}}{\partial \chi} \right)^2 h \dot{\lambda}_s^p + \\ + \frac{\partial \mathbf{f}}{\partial \boldsymbol{\sigma}} : \mathbf{E} : \left[(\llbracket \dot{\mathbf{u}} \rrbracket \otimes \mathbf{n}_b)^s - \dot{\lambda}_b^p \frac{\partial \mathbf{f}}{\partial \boldsymbol{\sigma}} \right] \delta_{\Sigma_b} - \left(\frac{\partial \mathbf{f}}{\partial \chi} \right)^2 h \dot{\lambda}_b^p \delta_{\Sigma_b} = 0. \end{aligned} \quad (25)$$

Therefore, for the two case of non-localized deformation and elasto/plastic bifurcation the value of the plastic multipliers are, respectively:

$$\dot{\lambda}_s^p = \frac{\frac{\partial \mathbf{f}}{\partial \boldsymbol{\sigma}} : \mathbf{E} : \dot{\boldsymbol{\varepsilon}}}{\frac{\partial \mathbf{f}}{\partial \boldsymbol{\sigma}} : \mathbf{E} : \frac{\partial \mathbf{f}}{\partial \boldsymbol{\sigma}} + \left(\frac{\partial \mathbf{f}}{\partial \chi} \right)^2 h}, \quad \dot{\lambda}_b^p = \frac{\frac{\partial \mathbf{f}}{\partial \boldsymbol{\sigma}} : \mathbf{E} : (\llbracket \dot{\mathbf{u}} \rrbracket \otimes \mathbf{n}_b)^s}{\frac{\partial \mathbf{f}}{\partial \boldsymbol{\sigma}} : \mathbf{E} : \frac{\partial \mathbf{f}}{\partial \boldsymbol{\sigma}} + \left(\frac{\partial \mathbf{f}}{\partial \chi} \right)^2 h}. \quad (26)$$

In order to evaluate the intrinsic dissipation in the whole structure Ω , we have to integrate in the spatial domain the expression (15), taking into account the definition of the plastic multiplier (20). In the case elasto/plastic bifurcation the intrinsic dissipation assumes the following expression:

$$\mathbb{D} = \int_{\Omega} \sigma_0 \dot{\lambda}_b^p \delta_{\Sigma_b} dV = \int_{\Sigma_b} \sigma_0 \dot{\lambda}_b^p 2w_b dS. \quad (27)$$

5. The phase-field model for strain localization

The aim of the present section is to regularize the problem of strain localization in plasticity according to a phase-field approach. In particular, in a structure $\Omega = \Omega_s \cup \Omega_b$ constituted by a quasi-brittle material, the localization of deformation is considered as a micro-structural change, described by the additional degree of freedom $c = c(\mathbf{x}, t)$, which coincides with the phase-field variable (see Fig. 1 (b)). The phase-field variable $c \in [0, 1]$ and equals 1 at the center of the localization band.

In the case of two or more phases occupying the volume of the structure Ω , the phase-field approach is applied to approximate the sharp interface between the different phases by means of a diffuse interface. To define the effective properties of the material, the most frequently applied homogenization assumptions are the Reuss/Sachs model and the Taylor/Voigt model (Ammar et al., 2009). The first model assumes that total strain is

spatially constant, while the latter assumes that the stress is spatially constant.

For the case of strain localization, some authors have adopted a sort of modified Reuss/Sachs model to homogenize the strain state by averaging the two phases strains, according to the following mixture law:

$$\boldsymbol{\varepsilon} = (1 - \beta) \boldsymbol{\varepsilon}_s + \beta \boldsymbol{\varepsilon}_b, \quad (28)$$

where β represents the volume fraction of the localization zone. The stress state is recovered making use of the principle of virtual works, considering that the work produced in the homogenized material must be equal to the volume-averaged work of the two phases (s, b), under the compatibility condition (28).

A different homogenization approach is reported in the paper of Pietruszczak and Mróz (1981), where a volume element containing the localization band is decomposed in two sub-elements connected in series. The first sub-element presents a rigid-plastic behavior, since the plastic deformation is concentrated in the localization band and the remaining part is assumed to be rigid. The latter sub-element is perfectly elastic. The plastic strain increment in the localization band is smeared over the whole element and the total strain increment assumes the following expression:

$$\dot{\boldsymbol{\varepsilon}} = \dot{\boldsymbol{\varepsilon}}^e + \beta \dot{\boldsymbol{\varepsilon}}_b^p, \quad (29)$$

with the stress state related to the elastic strain by the generalized Hooke's law.

In the present study, the homogenization is based on the kinematics of the interphase model (Giambanco and Mróz, 2001; Giambanco et al., 2012). With reference to the interphase volume element, depicted in Fig. 3, the total strain is decomposed into internal and external (contact) components. The internal strains are continuous, while the contact strains suffer discontinuity at the interphase:

$$\boldsymbol{\varepsilon}_b = \boldsymbol{\varepsilon}_b^i + \boldsymbol{\varepsilon}_b^c, \quad \llbracket \boldsymbol{\varepsilon}_b^c \rrbracket = (\mathbf{g} \otimes \mathbf{n})^s. \quad (30)$$

Therefore, the regularization of the discontinuous strain field can be viewed as the approximation of the interphase contact strain in the whole body Ω , making use of a specific weak Dirac delta function:

$$\boldsymbol{\varepsilon} = \hat{\boldsymbol{\varepsilon}} + \gamma(c, \nabla c) (\mathbf{g} \otimes \mathbf{n})^s, \quad (31)$$

where the strain jump, defined on the middle surface of the contact layer Σ_b , is regularized in the framework of the

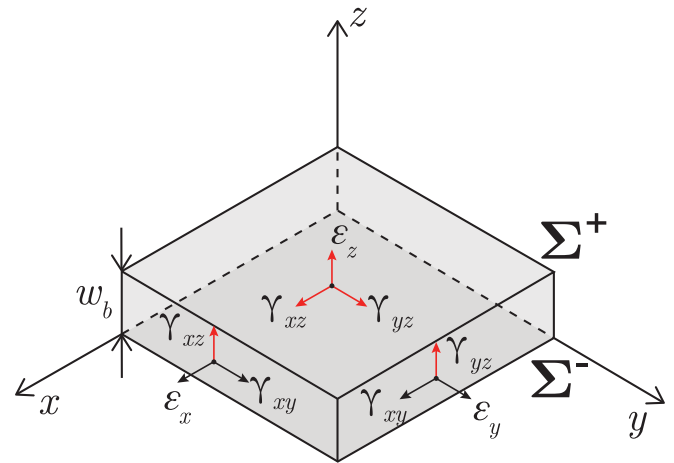


Fig. 3. Schematic representation of the kinematics at the interphase/plastic band: internal strains (black) are continuous while contact strains (red) are discontinuous. (For interpretation of the references to color in this figure legend, the reader is referred to the web version of this article.)

phase-field approach, employing the following Mumford–Shah type functional:

$$\gamma(c, \nabla c) = \frac{1}{2}(c^2 + w_b^2 |\nabla c|^2). \quad (32)$$

Taking advantage of the results carried out in the previous section, the inelastic strain and the kinematic internal variable can be defined as follows:

$$\boldsymbol{\varepsilon}^p := \boldsymbol{\varepsilon}_s^p + \gamma(c, \nabla c) \boldsymbol{\varepsilon}_b^p, \quad \xi := \xi_s + \gamma(c, \nabla c) \xi_b, \quad (33)$$

where it is straightforward to consider

$$\boldsymbol{\varepsilon}_b^p = (\mathbf{g} \otimes \mathbf{n})^s = \frac{1}{w_b} (\llbracket \mathbf{u} \rrbracket \otimes \mathbf{n}_b)^s. \quad (34)$$

5.1. Equilibrium

In a first gradient theory, the classical small strain tensor $\boldsymbol{\varepsilon}$ is accompanied by the microstrain vector $\boldsymbol{\delta}$ associated to the phase change, therefore, the kinematic compatibility equations are:

$$\boldsymbol{\varepsilon} = \nabla^s \mathbf{u}, \quad \boldsymbol{\delta} = \nabla c, \quad (35)$$

being ∇ the gradient operator and where the apex s indicates its symmetric part.

The boundary of the structure is divided in two parts Γ_u and Γ_t , where kinematic and loading conditions are specified, respectively. The external actions are the body force \mathbf{f} for unit volume and the surface tractions \mathbf{t} . Following Gurtin (1996), we postulate that there exists a micro-forces system characterized by an internal micro-force π and a micro-stress $\boldsymbol{\zeta}$, which are conjugated to the phase-field and its gradient, respectively.

The equilibrium of the structure can be expressed in the form of the Principle of Virtual Powers (PVP)

$$\int_{\Omega} (\boldsymbol{\sigma} : \dot{\boldsymbol{\varepsilon}} + \boldsymbol{\zeta} \cdot \dot{\boldsymbol{\delta}} - \pi \dot{c}) dV = \int_{\Omega} \mathbf{f} \cdot \dot{\mathbf{u}} dV + \int_{\Gamma_t} \mathbf{t} \cdot \dot{\mathbf{u}} dS \quad (36)$$

and it assesses that the internal work equals the external one for any virtual change of the configuration, i.e. that satisfies the kinematic compatibility Eq. (16). Substituting the kinematic compatibility equations in the PVP and applying the divergence theorem, we obtain:

$$\begin{aligned} & \int_{\Gamma_t} (\boldsymbol{\sigma} \mathbf{n} - \mathbf{t}) \cdot \dot{\mathbf{u}} dS + \int_{\Gamma} \boldsymbol{\zeta} \cdot \mathbf{n} \dot{c} dS + \\ & - \int_{\Omega} (\operatorname{div} \boldsymbol{\sigma} + \mathbf{f}) \cdot \dot{\mathbf{u}} dV - \int_{\Omega} (\operatorname{div} \boldsymbol{\zeta} + \pi) \cdot \dot{c} dV = 0, \end{aligned} \quad (37)$$

and, since the equality has to be verified for any configuration change, we derive the equilibrium equation and the corresponding boundary conditions associated to the displacement and phase changes, respectively:

$$\operatorname{div} \boldsymbol{\sigma} + \mathbf{f} = 0 \quad \text{in } \Omega, \quad \boldsymbol{\sigma} \mathbf{n} = \mathbf{t} \quad \text{on } \Gamma_t, \quad (38)$$

$$\operatorname{div} \boldsymbol{\zeta} + \pi = 0 \quad \text{in } \Omega, \quad \boldsymbol{\zeta} \cdot \mathbf{n} = 0 \quad \text{on } \Gamma. \quad (39)$$

5.2. Constitutive equations

In order to derive the constitutive equations of the phase-field mechanical model, let us consider the Clausius–Duhem instantaneous dissipation expressed as the difference of the time increment of the internal work and the time increment of the Helmholtz free energy:

$$\dot{D} = \boldsymbol{\sigma} : \dot{\boldsymbol{\varepsilon}} + \boldsymbol{\zeta} \cdot \dot{\boldsymbol{\delta}} - \pi \dot{c} - \dot{\psi} \geq 0, \quad (40)$$

being ψ the free energy, having the following general form:

$$\psi = \psi^e(\boldsymbol{\varepsilon}, \boldsymbol{\varepsilon}_p, c, \nabla c) + \psi^i(\xi, c, \nabla c). \quad (41)$$

Recalling the positions (32), the elastic and intrinsic parts of the free energy (41) assume the following forms

$$\psi^e = \frac{1}{2} (\boldsymbol{\varepsilon} - \boldsymbol{\varepsilon}_s^p - \gamma \boldsymbol{\varepsilon}_b^p) : \mathbf{E} : (\boldsymbol{\varepsilon} - \boldsymbol{\varepsilon}_s^p - \gamma \boldsymbol{\varepsilon}_b^p), \quad (42a)$$

$$\psi^i = \frac{1}{2} h(\xi_s + \gamma \xi_b)^2. \quad (42b)$$

Substituting the time increment of the free energy and the kinematic compatibility equations in the dissipation inequality (40), we have:

$$\begin{aligned} \dot{D} = & \left(\boldsymbol{\sigma} - \frac{\partial \psi^e}{\partial \boldsymbol{\varepsilon}} \right) : \nabla^s \dot{\mathbf{u}} + \left(\boldsymbol{\zeta} - \frac{\partial \psi^e}{\partial \nabla c} - \frac{\partial \psi^i}{\partial \nabla c} \right) \cdot \nabla \dot{c} \\ & - \frac{\partial \psi^e}{\partial \boldsymbol{\varepsilon}_s^p} : \dot{\boldsymbol{\varepsilon}}_s^p - \frac{\partial \psi^e}{\partial \boldsymbol{\varepsilon}_b^p} : \dot{\boldsymbol{\varepsilon}}_b^p + \\ & - \frac{\partial \psi^i}{\partial \xi_s} \dot{\xi}_s - \frac{\partial \psi^i}{\partial \xi_b} \dot{\xi}_b - \left(\pi + \frac{\partial \psi^e}{\partial c} + \frac{\partial \psi^i}{\partial c} \right) \dot{c} \geq 0. \end{aligned} \quad (43)$$

The instantaneous dissipation in presence of elasto/plastic bifurcation ($\dot{\boldsymbol{\varepsilon}}_s^p = \mathbf{0}$, $\dot{\xi}_s = 0$) is given by

$$\begin{aligned} \dot{D} = & \left(\boldsymbol{\sigma} - \frac{\partial \psi^e}{\partial \boldsymbol{\varepsilon}} \right) : \nabla^s \dot{\mathbf{u}} + \left(\boldsymbol{\zeta} - \frac{\partial \psi^e}{\partial \nabla c} - \frac{\partial \psi^i}{\partial \nabla c} \right) \cdot \nabla \dot{c} - \frac{\partial \psi^e}{\partial \boldsymbol{\varepsilon}_b^p} : \dot{\boldsymbol{\varepsilon}}_b^p \\ & - \frac{\partial \psi^i}{\partial \xi_b} \dot{\xi}_b - \left(\pi + \frac{\partial \psi^e}{\partial c} + \frac{\partial \psi^i}{\partial c} \right) \dot{c} \geq 0, \end{aligned} \quad (44)$$

which is linear in $\nabla^s \dot{\mathbf{u}}$ and $\nabla \dot{c}$. To ensure that the second law is satisfied in all conceivable processes and for any given thermodynamic variables, following the Coleman and Noll procedure (Coleman and Noll, 1963; Coleman and Gurtin, 1967), the analysis of the dissipation inequality leads to the following state laws:

$$\boldsymbol{\sigma} = \frac{\partial \psi^e}{\partial \boldsymbol{\varepsilon}} = \mathbf{E} : (\boldsymbol{\varepsilon} - \boldsymbol{\varepsilon}_s^p - \gamma \boldsymbol{\varepsilon}_b^p), \quad (45)$$

$$\boldsymbol{\zeta} = \frac{\partial \psi^e}{\partial \nabla c} + \frac{\partial \psi^i}{\partial \nabla c} = -w_b^2 (\boldsymbol{\sigma} : \boldsymbol{\varepsilon}_b^p - \chi \xi_b) \nabla c, \quad (46)$$

where the following position has been made

$$\chi := h(\xi_s + \gamma \xi_b). \quad (47)$$

Substituting Eqs. (45)–(47) in the expression of the instantaneous dissipation (44), we obtain:

$$\dot{D} = \gamma (\boldsymbol{\sigma} : \dot{\boldsymbol{\varepsilon}}_b^p - \chi \dot{\xi}_b) + \pi_{dis} \dot{c} \geq 0, \quad (48)$$

being π_{dis} the internal micro-force which contributes to the dissipation:

$$\pi_{dis} := -\pi - \frac{\partial \psi^e}{\partial c} - \frac{\partial \psi^i}{\partial c} = (\boldsymbol{\sigma} : \boldsymbol{\varepsilon}_b^p - \chi \xi_b) c - \pi. \quad (49)$$

Finally, for the case of non localized deformation ($\nabla \dot{c} = \mathbf{0}$, $\dot{\boldsymbol{\varepsilon}}_b^p = \mathbf{0}$, $\dot{\xi}_b = \dot{c} = 0$) the instantaneous dissipation assumes the form (9) where the increments of the elastoplastic strain and of the kinematic internal variable have to be referred to sound material (s).

5.3. Principle of maximum of instantaneous dissipation and flow rules

The instantaneous dissipation, obtained for the case of regularized localization (48), is additively decomposed in the dissipation developing in the plastic band, smeared on the whole volume of the structure, and in the dissipation related to the phase-change:

$$\dot{D} = \gamma \dot{D}_b^p + \dot{D}^{ph} \geq 0. \quad (50)$$

The principle of maximum dissipation, in this case, is the maximization of the functional (50) under the plasticity admissibility condition (11) and an additional condition, related to the phase change mechanism, with limit function depending on the dissipative micro-force:

$$\Phi^{ph}(\pi_{dis}) = \pi_{dis} - \pi_0 \leq 0, \quad (51)$$

where π_0 is the threshold value for the phase change.

The flow rules and the Kuhn–Tucker conditions derive from the following problem

$$\min_{\dot{\lambda}^p, \dot{\lambda}^c} \max_{\sigma, \chi} L(\dot{\epsilon}_b^p, \dot{\xi}_b, \dot{\lambda}^p, \dot{\lambda}^{ph}) = \gamma (\sigma : \dot{\epsilon}_b^p - \chi \dot{\xi}_b) + \pi_{dis} \dot{c} - \dot{\lambda}^p \Phi^p(\sigma, \chi) - \dot{\lambda}^{ph} \Phi^{ph}(\pi_{dis}) \quad (52)$$

where $\dot{\lambda}^{ph}$ is the phase-field multiplier. The solution of the problem (52) is

$$\frac{\partial L}{\partial \sigma} = 0 \rightarrow \gamma \dot{\epsilon}_b^p = \dot{\lambda}^p \frac{\partial \Phi^p}{\partial \sigma}, \quad (53a)$$

$$\frac{\partial L}{\partial \chi} = 0 \rightarrow \gamma \dot{\xi}_b = -\dot{\lambda}^p \frac{\partial \Phi^p}{\partial \chi}, \quad (53b)$$

$$\frac{\partial L}{\partial \pi_{dis}} = 0 \rightarrow \dot{c} = \dot{\lambda}^{ph} \frac{\partial \Phi^{ph}}{\partial \pi_{dis}}, \quad (53c)$$

with the loading/unloading conditions

$$\Phi^p(\sigma, \chi) \leq 0, \quad \dot{\lambda}^p \geq 0, \quad \Phi^p \dot{\lambda}^p = 0, \quad (54a)$$

$$\Phi^{ph}(\pi) \leq 0, \quad \dot{\lambda}^{ph} \geq 0, \quad \Phi^{ph} \dot{\lambda}^{ph} = 0. \quad (54b)$$

Substituting the flow rules in the expression of the instantaneous dissipation, we have

$$\dot{D} = \gamma \sigma_0 \dot{\lambda}_b^p + \pi_0 \dot{\lambda}^{ph}, \quad (55)$$

where it has been considered from Eqs. (52) and (53a) that $\gamma \dot{\lambda}_b^p = \dot{\lambda}^p$.

For the case of elastoplastic bifurcation, the total instantaneous dissipation in the body Ω must be equal to the instantaneous dissipation developed in the localization band, hence, the following equality has to be verified:

$$\int_{\Sigma_b} w_b \sigma_0 \dot{\lambda}_b^p dS = \int_{\Omega} (\gamma \sigma_0 \dot{\lambda}_b^p + \pi_0 \dot{\lambda}^{ph}) dV. \quad (56)$$

Remembering the property of the weak Dirac delta functional $\gamma(c, \nabla c)$, we can make the following position

$$\int_{\Omega} \frac{\gamma}{w_b} \sigma_0 \dot{\lambda}_b^p dV = \int_{\Sigma_b} \sigma_0 \dot{\lambda}_b^p dS, \quad (57)$$

and substituting in the balance Eq. (56) we obtain

$$\int_{\Omega} \pi_0 \dot{\lambda}^{ph} dV = 0, \quad (58)$$

with the trivial solution $\pi_0 = 0$.

This result, together with the expression (55), asserts that the phase change does not produce an increment of the instantaneous dissipation or it means that the regularization approach does not affect the mechanical problem in terms of energy dissipated.

Since the limit phase-field condition (51) reduces to

$$\Phi^{ph} = (\sigma : \dot{\epsilon}_b^p - \chi \dot{\xi}_b) c - \pi \leq 0, \quad (59)$$

the micro-force π is updated during the strain localization process, in order to satisfy (59) as equality, and the irreversibility of the phenomenon is satisfied, since the micro-force assumes the maximum of the values registered along the time history. Substituting

the expressions of the micro-force π , derived by the limit condition (59), and of the micro stress ξ (46) in the equilibrium Eq. (39), the following Ginzburg–Landau type differential equation results:

$$\Delta c - \alpha^2 c = 0, \quad (60)$$

where Δc is the Laplacian of the phase-field and $\alpha = \frac{1}{w_b}$.

6. Examples

To illustrate the performance of the proposed phase-field model, we present two examples of failure simulations of quasi-brittle structures. The first example illustrates the uniaxial response of a 1D bar under tension and it makes a comparison with respect to other solutions obtained without or with different strain homogenization. The second example, instead, illustrates the analysis of the three-point bending beam test, then a comparison with the experimental results obtained by Grégoire et al. (2013) is preformed.

In both cases the constitutive behavior of the plastic zone is described by the simplest stress–strain law with softening, based on the linear relation between stress and strain in the post-peak range, from the limit elastic strain ε_0 to a certain failure strain ε_f (see Fig. 4)

$$\sigma = \begin{cases} E\varepsilon & \text{if } 0 \leq \varepsilon \leq \varepsilon_0 \\ S(\varepsilon_f - \varepsilon) & \text{if } \varepsilon_0 \leq \varepsilon \leq \varepsilon_f \\ 0 & \text{if } \varepsilon \geq \varepsilon_f \end{cases} \quad (61)$$

where S is the parameter governing softening

$$S = -\frac{Eh}{E + h}. \quad (62)$$

6.1. Bar in tension

Fig. 5 shows a bar of Young's Modulus E , cross section A and length l , loaded in tension by a force F at the right end. The displacement of the left end is constrained. The response remains linearly elastic up to $u = u_0 = l\varepsilon_0$. At this state, the force F transmitted by the bar reaches its maximum value, $F_0 = A\sigma_0$. After that, the material exhibits a softening elasto-plastic response in the zone of length w_b (defect). At each cross section, the stress decreases either at increasing strain, by softening in the localization band, or at decreasing strain, by elastic unloading in the sound region having length $l_s = l_1 + l_2$. Firstly, this problem is approached considering the strain discontinuous with continuous displacement field in the localization band. In this sense, this analysis is named *discontinuous strain* (DS) model. Then, the localization band is smeared over the volume and the effective strain/stress is obtained by averaging the corresponding stress/strain in the localized and not localized regions. This analysis is named *homogenized strain/stress* (HS) model. Lastly, the proposed phase-field (PF) approach is used to regularize the discontinuous strain field (Eq. (31)).

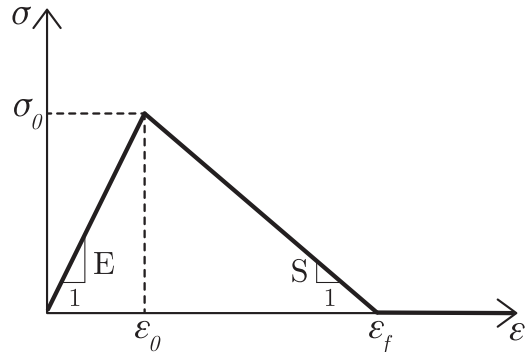


Fig. 4. Constitutive response of the localization band with linear softening curve.

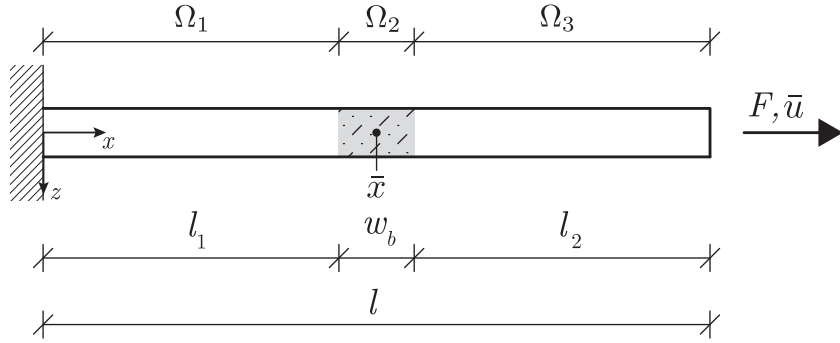


Fig. 5. Bar under uniaxial tension.

6.1.1. Discontinuous strain model

Considering the three domains $\Omega_1: [0 \leq x \leq l_1]$, $\Omega_2: [l_1 \leq x \leq l_1 + w_b]$, $\Omega_3: [l_1 + w_b \leq x \leq l]$ illustrated in Fig. 5, the standard axial second-order differential equation reads

$$u_i'' = 0 \quad \text{on } \Omega_i \text{ with } i = 1, 2, 3 \quad (63)$$

where the apex represents the derivative of the displacement u with respect to the abscissa x . The solution of (63) is obtained under the kinematic boundary conditions, the continuity of displacement field and the uniformity of stress distribution conditions

$$\begin{aligned} u_1(0) &= 0, \quad u_1(l_1) = u_2(l_1), \\ u_2(l_1 + w_b) &= u_3(l_1 + w_b), \quad u_3(l) = \bar{u}, \end{aligned} \quad (64a)$$

$$\sigma_1(l_1) = \sigma_2(l_1), \quad \sigma_2(l_1 + w_b) = \sigma_3(l_1 + w_b). \quad (64b)$$

Thus, including the constitutive Eq. (61), the strain field is determined

$$\begin{aligned} \varepsilon_1 = \varepsilon_3 &= \frac{S(\bar{u} - w_b \varepsilon_f)}{Sl - w_b(E + S)} \quad \text{on } \Omega_1, \Omega_3, \\ \varepsilon_2 &= \frac{E\bar{u} - \varepsilon_f S(l - w_b)}{w_b(E + S) - lS} \quad \text{on } \Omega_2. \end{aligned} \quad (65)$$

Since $E\varepsilon_0 = S(\varepsilon_f - \varepsilon_0)$, the strain jump $[\varepsilon]$ reads

$$[\varepsilon] = \frac{(\varepsilon_0 - \frac{\bar{u}}{l})}{\varepsilon_0 - \beta \varepsilon_f} \varepsilon_f, \quad (66)$$

where β is the fraction volume of the localization zone $\beta = w_b \setminus l$.

The stress evaluated at the end of the bar is

$$\sigma = \frac{\beta \varepsilon_f - \frac{\bar{u}}{l}}{\beta \varepsilon_f - \varepsilon_0} \sigma_0, \quad (67)$$

from which the tangent modulus of the descending branch in the load displacement diagram can be obtained

$$\frac{dF}{d\bar{u}} = \frac{EA}{l} \frac{\bar{\beta}}{\bar{\beta} - \beta} \quad (68)$$

where the dimensionless ratio $\bar{\beta}$ is equal to $\varepsilon_0 \setminus \varepsilon_f$. The case of $\varepsilon_f = \varepsilon_0$ corresponds to the brittle model while for increasing ε_f a more ductile behavior is obtained. Therefore, $\bar{\beta}$ can be called the brittleness number and its value is between 0 and 1. Hence, two conditions, related to the sign of the slope (68), can be distinguished

$$\text{if } \beta > \bar{\beta} \Rightarrow \frac{dF}{d\bar{u}} < 0, \quad (69)$$

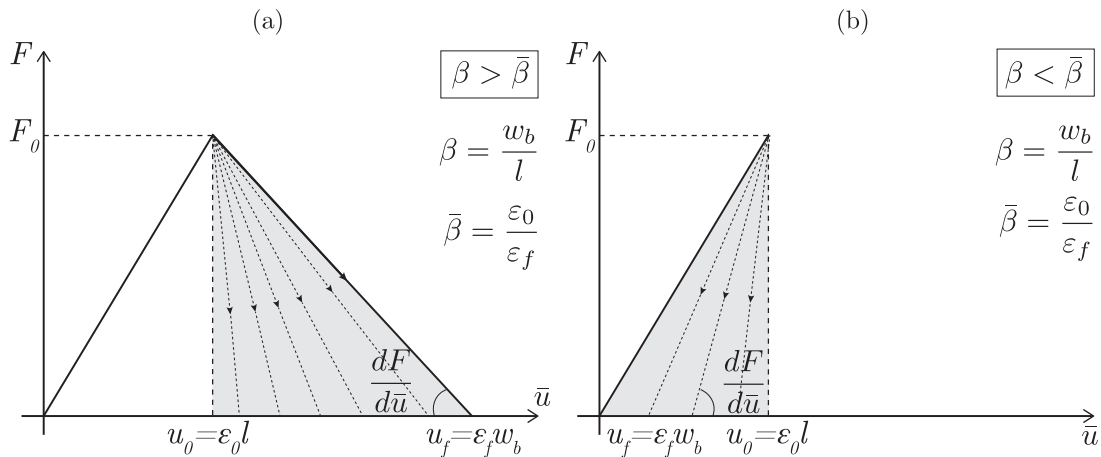
that is equal to $u_f = w_b \varepsilon_f = \beta u_0 / \bar{\beta} > u_0$. In this case the tangent modulus (68) is negative and the load-displacement diagram is the one shown in Fig. 6 (a). Conversely,

$$\text{if } \beta < \bar{\beta} \Rightarrow \frac{dF}{d\bar{u}} > 0, \quad (70)$$

condition that implies the positivity of the slope (68), i.e. the load-displacement diagram exhibits a snapback with $u_f < u_0$, as shown in Fig. 6 (b).

By considering Eq. (66) as a function of both β and $\bar{\beta}$, if condition (69) is valid, both numerator and denominator are negative, while if condition (70) is valid, both numerator and denominator are positive.

Remark 1. The strain jump $[\varepsilon]$ between the process zone and the sound zone is always positive.

Fig. 6. Load-displacement diagram in the cases (a) $\beta > \bar{\beta}$ and (b) $\beta < \bar{\beta}$

The two coefficients β and $\bar{\beta}$ represent the geometrical and the constitutive parameters that governs the response, $\beta = \bar{\beta}$ represents an undetermined case correspondent to the situation in which the strain-softening slope becomes vertical.

6.1.2. Homogenized strain/stress model

The 1D problem presented is here particularized considering that the average strain can be expressed as a combination of the inside-band and outside-band strain, following expression (28)

$$\varepsilon = (1 - \beta)\varepsilon_s + \beta\varepsilon_b, \quad (71)$$

being valid

$$\varepsilon_b - \varepsilon_s = \frac{[u]}{l}, \quad (72)$$

with $[u]$ representing the displacement jump between the sound and the process zone. The stress can be also expressed as the weighted-average of the inside-band and outside-band stresses, as the Voigt/Taylor homogenization (Nguyen et al., 2016)

$$\sigma = (1 - \beta)\sigma_s + \beta\sigma_b, \quad (73)$$

where σ_s and σ_b are obtained according to the constitutive conditions of linear elasticity and softening inside and outside the localization zone

$$\sigma_s = E\varepsilon_s, \quad \sigma_b = S(\varepsilon_f - \varepsilon_b). \quad (74)$$

Using the stress continuity relation $\sigma_s = \sigma_b$ together with Eqs. (71), (72) and (74), the strain jump can be obtained as

$$\frac{[u]}{l} = \frac{\beta[S\varepsilon_f - (E + S)\varepsilon]}{S(1 - \beta) - E\beta}, \quad (75)$$

and may be introduced in (73) with the values of ε_s and ε_b obtained from Eqs. (71), (72) and the constitutive relations (74), yielding

$$\sigma = \frac{ES(\varepsilon - \beta\varepsilon_f)}{S - \beta(E + S)}. \quad (76)$$

In this case, the elastic line Eq. (63) gives a linear displacement distribution on the whole domain Ω : $[0 \leq x \leq l]$, under the kinematic boundary conditions (64a)₁ and (64a)₄, and a constant strain field on the whole domain. Thus, the stress along the bar reads

$$\sigma = \frac{\beta\varepsilon_f - \frac{\bar{u}}{l}}{\beta\varepsilon_f - \varepsilon_0} \sigma_0, \quad (77)$$

that coincides with Eq. (67) of the DS model. The force-displacement response does not differ from that analyzed by the DS model.

6.1.3. Phase-field model

The mechanical governing Eq. (38)_a together with the state law (45) with a linear elastic behavior outside the localized band ($\varepsilon_s^p = 0$), lead to the following differential equation

$$u_x'(x) = \frac{F}{EA} + \varepsilon_b^p \gamma(c), \quad \text{in } \Omega, \quad (78)$$

subjected to the kinematical condition $u_x = 0$ at $x = 0$. On the other hand, in view of the phase-equilibrium Eq. (39)_a with the state law (46) and the flow rules (53a), (53b), the limit conditions (54a) and (59), the Ginzburg-Landau differential equation is

$$c''(x) - \alpha^2 c(x) = 0, \quad \text{in } \Omega, \quad (79)$$

with $\alpha = 1/w_b$.

The solution of (79) gives

$$c(x) = e^{-\alpha|x-\bar{x}|}, \quad (80)$$

which approaches 1 at the center of the localization band, $c(\bar{x}) = 1$, and vanishes far away from the band, $c(\pm\infty) = 0$. The Mumford-Shah functional assumes the following form

$$\gamma(c) = c(x)^2. \quad (81)$$

Substituting Eq. (81) in Eq. (78) and solving the differential equation we have

$$u_x(x) = \frac{Fx}{EA} + \varepsilon_b^p (\mathcal{I} - \mathcal{I}_0), \quad \text{in } \Omega, \quad (82)$$

where \mathcal{I} is the antiderivative of Mumford-Shah functional $\gamma(c)$, which evaluated at $x = 0$ is \mathcal{I}_0

$$\mathcal{I} = \int \gamma(c) dx = \frac{1}{\alpha} \left(\mathcal{H}(x - \bar{x}) - \frac{1}{2} \text{sign}(x - \bar{x}) \gamma(c) \right), \quad (83)$$

being $\mathcal{H}(x)$ the Heaviside step function.

In Eq. (82), ε_b^p , equal to λ_b^p (flow rule (53a)), can be expressed as a function of the constitutive parameters and the applied force, combining Eqs. (78) and (61) at $x = \bar{x}$

$$\varepsilon_b^p = \lambda_b^p = \varepsilon_f - \frac{F(E + S)}{AES}. \quad (84)$$

Particularizing the displacement (82) at $x = l$ and considering Eq. (84), the bar stiffness is obtained

$$\frac{dF}{d\bar{u}} = \frac{EA}{l} \frac{\bar{\beta}}{\bar{\beta} - (\mathcal{I}_l - \mathcal{I}_0)/l} \quad (85)$$

where

$$\mathcal{I}_l - \mathcal{I}_0 = \int_0^l \gamma dx = w_b. \quad (86)$$

for $0 < \bar{x} < l$ and if the characteristic length of the localization band is much smaller than the characteristic length of the structure, hypothesis at the basis of the strain localization theory. Let us note that $\beta = (\mathcal{I}_l - \mathcal{I}_0)/l$ and Eq. (85) coincides with (68).

Now we considered a bar 83 mm long with a notch 3 mm wide in the middle, having yield stress equal to 3.24 MPa, secant modulus of elasticity $2.61 \cdot 10^4$ MPa, softening parameter -250 MPa. This specimen has been studied experimentally by Gopalaratnam and Shah (1985).

Since a monotonic loading history is adopted, the inability of plasticity models to describe the gradual reduction of the elastic stiffness experimentally observed during unloading, is considered irrelevant. Fig. 7 (a) and (b) illustrate the strain and displacement profiles along the bar according to the three models at the softening branch, when $\bar{u} = 0.03$ mm, (see Fig. 7 (c)).

6.2. Three point bending test

As another example of applicability of the proposed model, we present the analytical simulation of a three-point bending test performed by Grégoire et al. (2013) on concrete beams. Fig. 8 shows the simply supported beam of length l subject to a concentrated load F at its mid-point. The beam response is governed by the second order differential equation

$$u_z''(x) = \frac{F}{EI} \left[\mathcal{H}\left(x - \frac{l}{2}\right) \left(x - \frac{l}{2}\right) - \frac{x}{2} \right] - \gamma(c) \varphi_b^p \quad (87)$$

being φ_b^p the plastic band curvature and I the cross section moment of inertia. Since the problem is uniaxial, it is noted that the Ginzburg-Landau differential equation is the same of the previous example.

From the boundary conditions $u_z = 0$ at $x = 0$ and $x = l$, it follows the displacement field expression

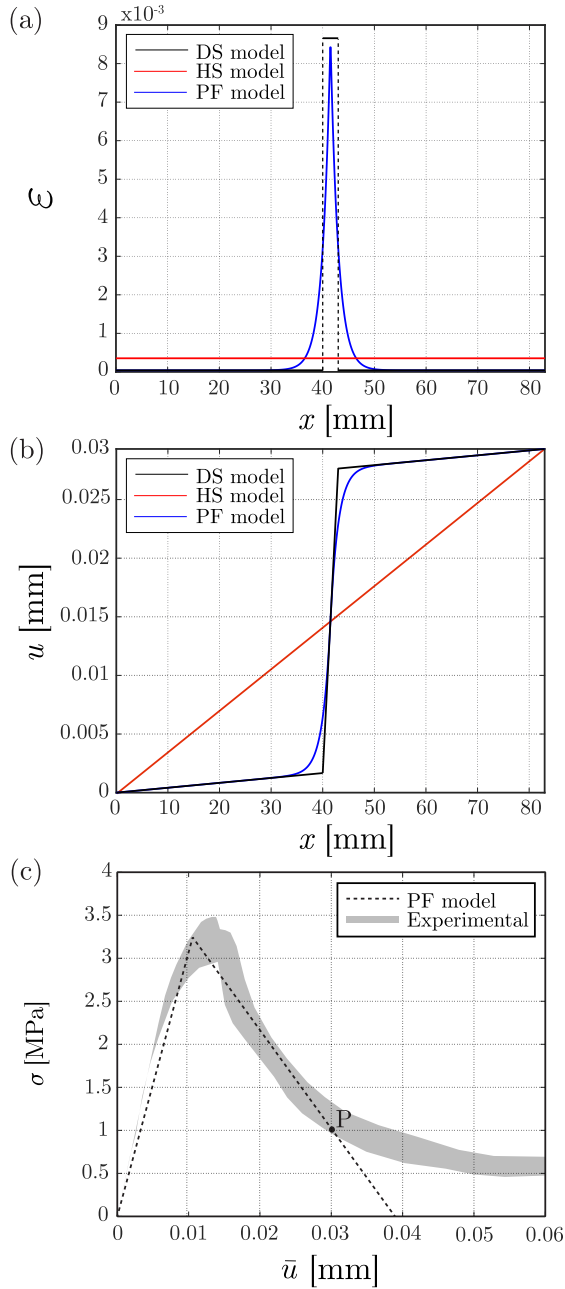


Fig. 7. Tensile test on a mortar bar performed by Gopalaratnam and Shah (1985). Response in terms of (a) strain and (b) displacement for the discontinuous strain, homogenized strain and phase-field models, at point P of the (c) $\sigma - \bar{\epsilon}$ diagram.

$$u_z(x) = \frac{F}{EI} \left[\mathcal{H} \left(x - \frac{l}{2} \right) \frac{1}{6} \left(x - \frac{l}{2} \right)^3 - \frac{x^3}{12} + \frac{3l^2x}{48} \right] + \varphi_b^p \left[(\mathcal{I}I_l - \mathcal{I}I_0) \frac{x}{l} + \mathcal{I}I_0 - \mathcal{I}I \right], \quad (88)$$

where $\mathcal{I}I$ is the double integral of the Mumford–Shah functional

$$\mathcal{I}I = \iint \gamma(c) dx = \frac{1}{\alpha} \left(R(x - \bar{x}) + \frac{\gamma(c)}{4\alpha} \right) \quad (89)$$

that, evaluated at $x = 0$ and $x = l$, reads, respectively,

$$\mathcal{I}I_0 = \iint \gamma(c) dx \Big|_{x=0} = \frac{e^{-2\alpha\bar{x}}}{4\alpha^2}, \quad (90a)$$

$$\mathcal{I}I_l = \iint \gamma(c) dx \Big|_{x=l} = \frac{1}{\alpha} \left(\frac{e^{-2\alpha(l-\bar{x})}}{4\alpha} + l - \bar{x} \right), \quad (90b)$$

and $R(x - \bar{x})$ is the ramp function defined as

$$R(x - \bar{x}) = \mathcal{H}(x - \bar{x})(x - \bar{x}). \quad (91)$$

In Eq. (88), φ_b^p is evaluated considering the phase-field homogenization

$$\varphi^p := \varphi_s^p + \gamma \varphi_b^p \quad (92)$$

and the moment-curvature relation, which has been constructed by the analysis of the mid-span beam section subjected to bending. Three stages can be distinguished, as illustrated in Fig. 9, the elastic stage (Fig. 9 (a)), the softening stage before cracking (Fig. 9 (b)), and the cracking stage (Fig. 9 (c)). The ultimate elastic bending moment M_0 and the corresponding curvature φ_0 (point A in Fig. 10) can be calculated using the requirements of equilibrium of forces and strain compatibility

$$M_0 = \frac{BH^2}{6} f_t, \quad (93a)$$

$$\varphi_0 = \frac{2\epsilon_0}{H}, \quad (93b)$$

where f_t is the tensile strength of concrete, ϵ_0 is the ultimate elastic strain which characterizes the starting of the strain softening process. Beyond ϵ_0 , the tensile stress decreases linearly with increasing tensile strain ϵ_t (see Fig. 9 (b)). Then, failure takes place by cracking when tensile strain exceeds the value ϵ_f (Fig. 9 (c)). Thus, the strain ϵ_f is the fracture tensile strain which characterizes the end of the softening process when the micro-cracks coalesce into a continuous free-stress crack. At this point (point B in Fig. 10), the bending moment returns to the value of the ultimate elastic M_0 .

To determine the close-form moment-curvature relation for the section in the post-elastic regime, the basic assumption of

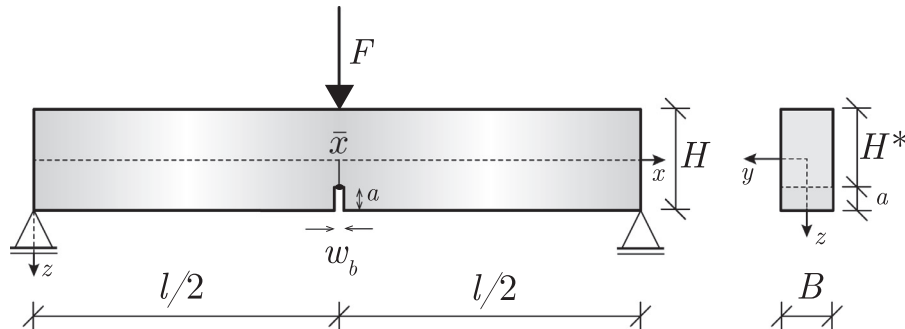


Fig. 8. Three point bending beam.

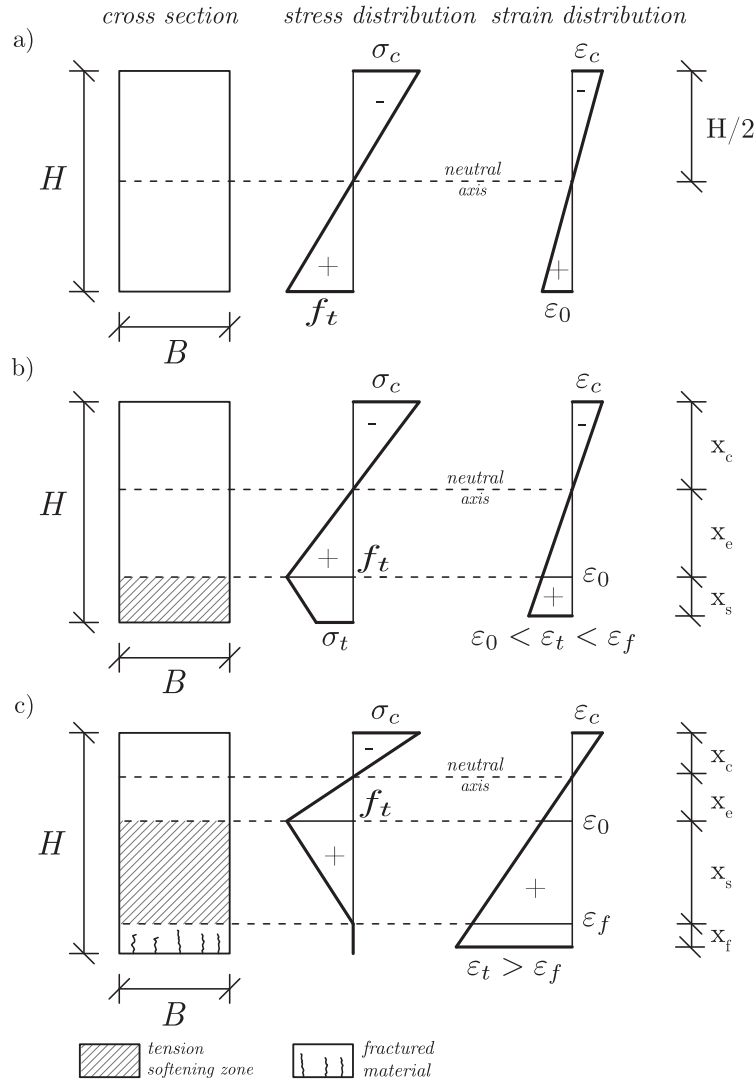


Fig. 9. Distribution of stress and strain along the cross section in bending at (a) ultimate elastic stage, (b) formation of a softening region, (c) formation of flexural cracks.

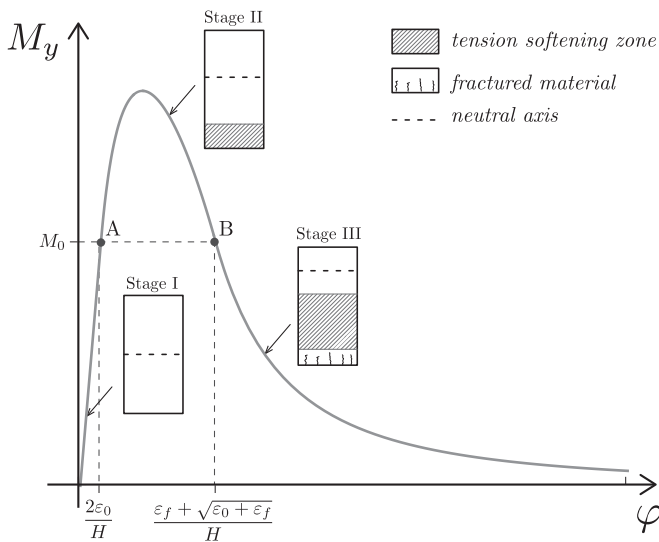


Fig. 10. Moment (M_y) - Curvature (φ) cross-section behavior.

plane sections was used, therefore, the strain in a generic point of the section is proportional to the distance from the neutral axis, in addition to that, the translational and the rotational equilibrium of the internal tension and compression are enforced.

Appendix A provides the equilibrium and the compatibility equations. Since the rotational equilibrium of the forces results in a nonlinear equation, the plastic curvature in the localization band is evaluated numerically.

In the bending test performed by Grégoire et al. (2013), the span length l is equal to 250 mm, the depth H measures 100 mm and the thickness B is 50 mm. The notch-to-depth (a/H) ratio of 0.2 was considered. The elastic parameter E used for the application is the average value provided by Grégoire et al. (2013), equal to 37 GPa. The band width was assumed to be equal to the internal length of the non-local model proposed by Grégoire et al. (2013), equal to 40 mm. Making use of Eq. (88), the force-midspan displacement diagram was calculated in order to fit the experimental data. The best fitting curve has been found with $\varepsilon_0 = 0.0676$, $\varepsilon_f = 1.1486$, Fig. 11 (a). In the same figure, (b) beam deflection, (c) plastic and (d) elastic curvature at the stage J, K, L of the load-displacement curve have been plotted. The load-displacement curve, compared with the experimental one of Grégoire et al. (2013) (red solid curve represents the mean value) shows that the model can sufficiently reproduce the experimental behavior. Consistently with the model, with increasing deflection, the plastic curvature increases in the localization band with a smooth transition between the localization and the sound material. The elastic curvature increases linearly from zero at the supports to a maximum at

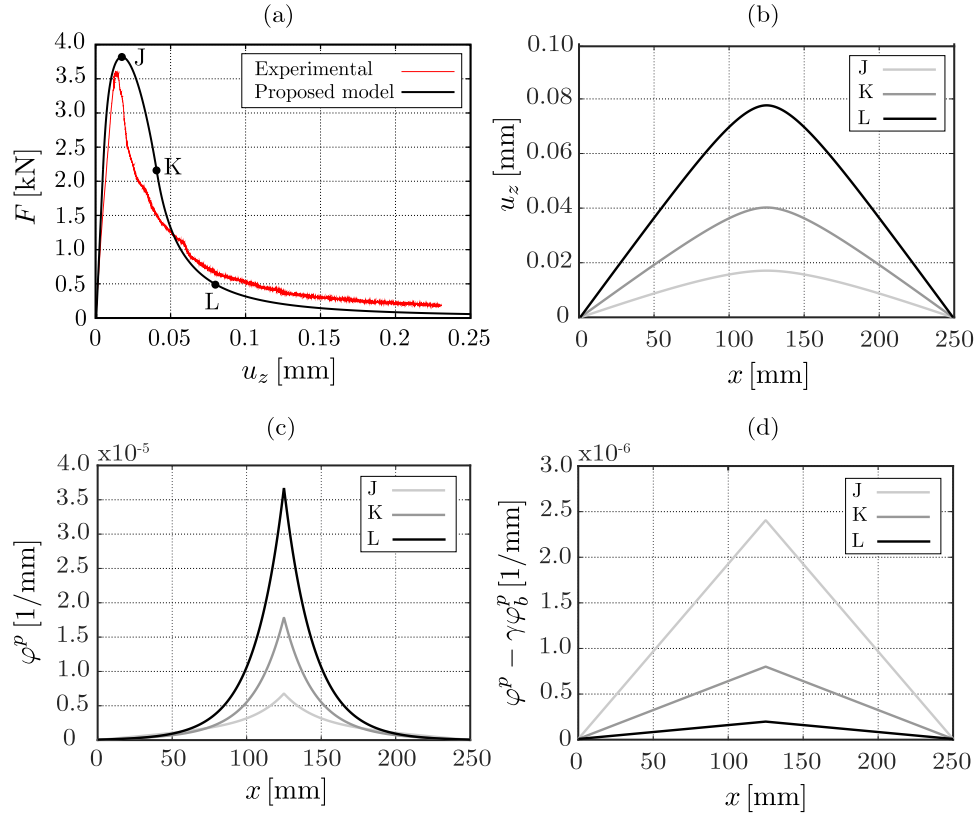


Fig. 11. Three point bending example. (a) Force as a function of the mid-span vertical displacement. The red curve is the average of the experimental data obtained by Grégoire et al. (2013). (b) Deflection, (c) Plastic curvature and (d) Elastic curvature of the beam at the point J, K, L of the load-displacement curve. (For interpretation of the references to color in this figure legend, the reader is referred to the web version of this article.)

the localization band which, instead, decreases with increasing deflection.

7. Conclusions

The well-known problem of strain localization in softening elastoplastic materials has been approached in the present work in an original way making use of the interphase model and the phase-field model theory. In particular, the narrow zone where strains concentrate is kinematically modeled using the interphase model and the phase-field variable has been introduced to regularize the contact strains at the interface between the plastic strain band and the surrounding material. This corresponds to diffuse the interphase in the volume of the solid body.

The theoretical treatment of the problem has been developed in a classical way making use of the principles of thermodynamics. With respect to other phase-field models applied to similar mechanical problems, the novelty consists in a Reuss/Sachs type homogenization of the inelastic contact strains through a weak Dirac delta function which, for a multi-axial problem, takes the shape of the Mumford-Shah functional. The introduction of this kinematical hypothesis naturally leads to the complete definition of the governing equations for a localized body.

The model has been tested by means of two 1D applications. The results show that (i) the introduced strain regularization does not affect substantially the structure behavior, (ii) the model can be easily used to replicate experimental results.

The authors believe that this general theory can be easily developed in different contexts as the strain localization in soil mechanics, plastic hinge formation in reinforced concrete frames and delamination in composite materials. Finally, a key point of the proposed model is that the calibration of model parameters for the

comparison between numerical and experimental results can be performed easily, since no additional mechanical parameters are required with respect to those that characterize the elastoplastic behavior.

Acknowledgments

A grant from the Italian Ministry for University and Research (MIUR) for PRIN-2015, project No. 2015LYXXA8, Multiscale mechanical models for the design and optimization of microstructured smart materials and metamaterials is gratefully acknowledged.

Appendix A. Moment-curvature relation for a section in the post-elastic regime

The translational and rotational equilibrium equations can be generally written as

$$\int_{A_t} \sigma_t dA = \int_{A_c} \sigma_c dA, \quad (\text{A.1a})$$

$$\frac{M_y}{B} = \int_{A_t} \sigma_t x dA + \int_{A_c} \sigma_c x dA. \quad (\text{A.1b})$$

where A_t and A_c represent the areas of concrete acted on by the tensile (σ_t) and compressive stresses (σ_c), respectively, and x the distance from the neutral axis. When the concrete section is subjected to softening (Fig. 9 (b)), Eqs. (A.1a) and (A.1b) can be particularized as

$$f_t(x_e + x_s) + \sigma_t x_s = \sigma_c x_c, \quad (\text{A.2a})$$

$$M_y = \frac{B}{6} (2\sigma_c x_c^2 + 2f_t x_e^2 + 3(f_t + \sigma_t) x_e x_s + (f_t + 2\sigma_t) x_s^2), \quad (\text{A.2b})$$

where x_c , x_e , x_s can be written for the plane sections as

$$x_c = \frac{\varepsilon_c}{\varepsilon_c + \varepsilon_t} H, \quad (\text{A.3a})$$

$$x_e = \frac{\varepsilon_0}{\varepsilon_c + \varepsilon_t} H, \quad (\text{A.3b})$$

$$x_s = \frac{\varepsilon_t - \varepsilon_0}{\varepsilon_c + \varepsilon_t} H, \quad (\text{A.3c})$$

and compressive and tensile stresses can be evaluated according to the constitutive equations

$$\sigma_c = E\varepsilon_c, \quad (\text{A.4a})$$

$$\sigma_t = S(\varepsilon_f - \varepsilon_t). \quad (\text{A.4b})$$

Lastly, the plastic curvature is calculated as the difference between the total and the elastic curvature

$$\varphi^p = \varphi - \varphi^e = \frac{\varepsilon_t}{H - x_c} - \frac{M_y}{EI}. \quad (\text{A.5})$$

When the formation of cracking is started (Fig. 9 (c)), Eqs. (A.2a) and (A.2b) simplify as

$$f_t(x_e + x_s) = \sigma_c x_c, \quad (\text{A.6a})$$

$$M_y = \frac{B}{6} (2\sigma_c x_c^2 + f_t(x_e + x_s)(2x_e + x_s)), \quad (\text{A.6b})$$

where x_c and x_c are evaluated as in Eqs. (A.3a) and (A.3b) while Eq. (A.3c) changes as

$$x_s = \frac{\varepsilon_f - \varepsilon_0}{\varepsilon_c + \varepsilon_t} H. \quad (\text{A.7})$$

References

- Alessi, R., Vidoli, S., Lorenzis, L.D., 2018. A phenomenological approach to fatigue with a variational phase-field model: the one-dimensional case. *Eng. Fract. Mech.* 190, 53–73. doi:10.1016/j.engfracmech.2017.11.036.
- Ambati, M., Gerasimov, T., De Lorenzis, L., 2015. Phase-field modeling of ductile fracture. *Comput. Mech.* 55 (5), 1017–1040. doi:10.1007/s00466-015-1151-4.
- Ammar, K., Appolaire, B., Cailletaud, G., Forest, S., 2009. Combining phase field approach and homogenization methods for modelling phase transformation in elastoplastic media. *Eur. J. Comput. Mech./Revue Européenne de Mécanique Numérique* 18 (5–6), 485–523.
- Benvenuti, E., Borino, G., Tralli, A., 2002. A thermodynamically consistent nonlocal formulation for damaging materials. *Eur. J. Mech. – A/Solids* 21 (4), 535–553. doi:10.1016/S0997-7538(02)01220-2.
- Borden, M., Verhoosel, C., Scott, M., Hughes, T., Landis, C., 2012. A phase-field description of dynamic brittle fracture. *Comput. Methods Appl. Mech. Eng.* 217–220, 77–95. doi:10.1016/j.cma.2012.01.008.
- Borino, G., Polizzotto, C., 2007. Thermodynamically consistent residual-based gradient plasticity theory and comparisons. *Model. Simul. Mater. Sci. Eng.* 15 (1), S23–S35. doi:10.1088/0965-0393/15/1/S03.
- Coleman, B., Gurtin, M., 1967. Thermodynamics with internal state variables. *J. Chem. Phys.* 47 (2), 597–613. doi:10.1063/1.1711937.
- Coleman, B., Noll, W., 1963. The thermodynamics of elastic materials with heat conduction and viscosity. *Arch. Ration. Mech. Anal.* 13 (1), 167–178. doi:10.1007/BF01262690.
- Feng, D., Wu, J., 2018. Phase-field regularized cohesive zone model (czm) and size effect of concrete. *Eng. Fract. Mech.* 197, 66–79. doi:10.1016/j.engfracmech.2018.04.038.
- Fileccia Scimemi, G., Giambanco, G., Spada, A., 2014. The interphase model applied to the analysis of masonry structures. *Comput. Methods Appl. Mech. Eng.* 279, 66–85. doi:10.1016/j.cma.2014.06.026.
- Francfort, G., Bourdin, B., Marigo, J.-J., 2008. The variational approach to fracture. *J. Elast.* 91 (1–3), 5–148. doi:10.1007/s10659-007-9107-3.
- Freddi, F., Royer Carfagni, G., 2016. Phase-field slip-line theory of plasticity. *J. Mech. Phys. Solids* 94, 257–272. doi:10.1016/j.jmps.2016.04.024.
- Giambanco, G., La Malfa Ribolla, E., Spada, A., 2014. CH of masonry materials via meshless meso-modeling. *Frattura ed Integrità Strutturale* (29) 150.
- Giambanco, G., La Malfa Ribolla, E., Spada, A., 2018. Meshless meso-modeling of masonry in the computational homogenization framework. *Meccanica* 53 (7), 1673–1697. doi:10.1007/s11012-017-0664-7.
- Giambanco, G., Mróz, Z., 2001. The interphase model for the analysis of joints in rock masses and masonry structures. *Meccanica* 36 (1), 111–130. doi:10.1023/A:1011957217840.
- Giambanco, G., Scimemi, G., Spada, A., 2012. The interphase finite element. *Comput. Mech.* 50 (3), 353–366. doi:10.1007/s00466-011-0664-8.
- Gopalratnam, V., Shah, S.P., 1985. Softening response of plain concrete in direct tension. *J. Am. Concr. Inst.* 82 (3), 310–323.
- Grégoire, D., Rojas-Solano, L.B., Pijaudier-Cabot, G., 2013. Failure and size effect for notched and unnotched concrete beams. *Int. J. Numer. Anal. Methods Geomech.* 37 (10), 1434–1452.
- Gurtin, M., 1996. Generalized Ginzburg-Landau and Cahn-Hilliard equations based on a microforce balance. *Physica D* 92 (3–4), 178–192. doi:10.1016/0167-2789(95)00173-5.
- Jirásek, M., 2001. Modeling of localized damage and fracture in quasibrittle materials. In: *Continuous and Discontinuous Modelling of Cohesive-Frictional Materials*. Springer, pp. 17–29.
- Miehe, C., Hofacker, M., Welschinger, F., 2010. A phase field model for rate-independent crack propagation: Robust algorithmic implementation based on operator splits. *Comput. Methods Appl. Mech. Eng.* 199 (45–48), 2765–2778. doi:10.1016/j.cma.2010.04.011.
- Moës, N., Dolbow, J., Belytschko, T., 1999. A finite element method for crack growth without remeshing. *Int. J. Numer. Methods Eng.* 46 (1), 131–150.
- Nguyen, G.D., Nguyen, C.T., Nguyen, V.P., Bui, H.H., Shen, L., 2016. A size-dependent constitutive modelling framework for localised failure analysis. *Comput. Mech.* 58 (2), 257–280.
- Ottosen, N., Runesson, K., 1991. Properties of discontinuous bifurcation solutions in elasto-plasticity. *Int. J. Solids Struct.* 27 (4), 401–421. doi:10.1016/0020-7683(91)90131-X.
- Palmer, A.C., Rice, J.R., 1973. The growth of slip surfaces in the progressive failure of over-consolidated clay. *Proc. R. Soc. A Math. Phys. Eng. Sci.* 332 (1591), 527–548.
- Pietruszczak, S., Mróz, Z., 1981. Finite element analysis of deformation of strainsoftening materials. *Int. J. Numer. Methods Eng.* 17 (3), 327–334. doi:10.1002/nme.1620170303.
- Rudnicki, J., Rice, J., 1975. Conditions for the localization of deformation in pressure-sensitive dilatant materials. *J. Mech. Phys. Solids* 23 (6), 371–394. doi:10.1016/0022-5096(75)90001-0.
- Simo, J., Oliver, J., Armero, F., 1993. An analysis of strong discontinuities induced by strain-softening in rate-independent inelastic solids. *Comput. Mech.* 12 (5), 277–296. doi:10.1007/BF00372173.
- Spada, A., Giambanco, G., La Malfa Ribolla, E., 2015. A FE-meshless multiscale approach for masonry materials. In: *Procedia Engineering*, 109, pp. 364–371. doi:10.1016/j.proeng.2015.06.244.
- Verhoosel, C., de Borst, R., 2013. A phase-field model for cohesive fracture. *Int. J. Numer. Methods Eng.* 96 (1), 43–62. doi:10.1002/nme.4553.
- Zhang, Z., Zheng, X., 2012. The representation of line dirac delta function along a space curve. *arXiv:1209.3221*